www.MaterialsViews.com

Subcompartmentalized Nanoreactors as Artificial Organelle with Intracellular Activity

*Bo Thingholm, Philipp Schattling, Yan Zhang, and Brigitte Städler**

Cell mimicry is an approach which aims at substituting missing or lost activity. In this context, the goal of artificial organelles is to provide intracellularly active nanoreactors to affect the cellular performance. So far, only a handful of reports discuss concepts addressing this challenge based on single-component reactors. Here, the assembly of nanoreactors equipped with glucose oxidase (GOx)-loaded liposomal subunits coated with a poly(dopamine) polymer layer and RGD targeting units is reported. When comparing different surface modifications, the uptake of the nanoreactors by endothelial cells and macrophages with applied shear stress is confirmed without inherent cytotoxicity. Furthermore, the encapsulation and preserved activity of GOx within the nanoreactors is shown. The intracellular activity is demonstrated by exposing macrophages with internalized nanoreactors to glucose and assessment of the cell viability after 6 and 24 h. The macrophage viability is found to be reduced due to the intracellularly produced hydrogen peroxide by GOx. This report on the first intracellular active subcompartmentalized nanoreactors is a considerable step in therapeutic cell mimicry.

1. Introduction

Nature has perfected the way our cells operate and function in our body. Multiple reactions happen in parallel, in a cascade manner, executed by highly specialized subunits under stringent control. The successful interplay between the nuclei as the carrier of the genetic information, the ribosome as the protein factory, and the mitochondria as the energy plant among others is what defines a healthy living organism. However, the treatment of malfunctioning organelles, either since birth or due to environmental factors, is challenging.[1]

Therapeutic cell mimicry (TCM) aims to substitute for missing or lost cellular function by imitating a specific cellular activity, i.e., by performing encapsulated biocatalysis to synthesize, degrade, or convert a specific compound in the required product. Since many diseases are related to the malfunctioning or missing of a specific enzyme, TCM might have the potential to provide a platform to address a variety of medical conditions. Enzyme replacement therapy as such is a well-known concept,[2] which faces a lot of challenges predominantly due to the loss of enzymatic function in biological environments. TCM is a nature-inspired approach that tries to mimic biological concepts to facilitate the interaction of synthetic assemblies (formulations) with biological systems in a sustained manner. Options are to mimic either the entire cells or their organelles. In the latter case, typically small single compartment systems, encapsulating one or more specific enzymes, are considered as simple mimics.[3] Among the most crucial aspects of artificial organelles is their ability to be active inside of a biological cell. However, only few published reports demonstrated intracellular activity using polymersomes or hollow silica nanospheres. Ben-Haim et al.[4] and later van Dongen et al.[5] demonstrated the uptake by cells and preserved activity of enzyme-loaded polymersomes within the cells, employing model systems. Tanner et al.[6] assembled a reactor that could combat oxidative stress in THP-1 cells via an encapsulated enzymatic

B. Thingholm, Dr. P. Schattling,
Dr. Y. Zhang, Dr. B. Städler
Interdisciplinary Nanoscience Center
Aarhus University
Gustav Wieds Vej 14, Aarhus 8000, Denmark
E-mail: bstadler@inano.au.dk

DOI: 10.1002/smll.201502109

cascade reaction. The group of Mou employed enzyme-loaded silica nanospheres for the triggered conversion of prodrugs.[7] These first reports highlight the potential of the approach to equip natural cells with artificial organelles toward a potential treatment of organelle dysfunction, but the field is in its infancy with a magnitude of scientific challenges to be overcome and fundamental aspects to be elucidated.

From a different perspective, the assembly of subcompartmentalized microreactors is a promising approach toward the creation of therapeutic artificial cells[8] Such microreactors mimic the hierarchical structure of a cell, which allow them to perform multiple reactions simultaneously in a spatially confined manner with high efficiency and accuracy. Subcompartmentalized systems have been fabricated using predominantly a combination of liposomes, polymersomes, and polymer capsules as building blocks.[9] Among the most advanced approaches are polymersomes in polymersomes[10] and capsosomes, liposomes within polymer carrier capsules,[11] including the demonstration of encapsulated enzymatic cascade reactions as the most complex functionality in both cases. Janus microreactors, toward the mimicry of the polarity of cells, were recently reported.[12] Furthermore, we advanced capsosomes toward their use as an oral treatment for phenylketonuria by loading them with the enzyme phenylalanine ammonialyase, which converts phenylalanine into benign *trans*-cinnamic acid in the intestine.[13] We demonstrated that such capsosomes could be used as extracellular microreactors with preserved activity in cell culture with applied peristaltic flow. Thus far, the concept of subcompartmentalization has never been considered for intracellular active reactors, although natural organelles contain separated subunits to facilitate parallel reactions while avoiding undesired interactions. Furthermore, free liposomes suffer from instability in biological environment. In contrast, we have recently demonstrated that capsosomes exhibit superior stability of the liposomal subunits when exposed to the enzyme phospholipase.[14] Therefore, subcompartmentalized artificial organelles might turn out to be superior over single compartment structures.

Herein, we report the assembly of subcompartmentalized nanoreactors with intracellular activity (**Scheme 1**). Specifically, we i) coated 800 nm silica particles with poly(dopamine) (PDA), poly(ethylene glycol) (PEG), or (arginylglycylaspartic acid) (RGD) and compared their uptake by endothelial cells and macrophages without and with applied shear stress, ii) assembled and characterized subcompartmentalized nanoreactors by depositing enzyme-loaded liposomal subunits onto the silica particles prior to the surface-modification with RGD, and iii) confirmed their intracellular enzymatic activity by the production of hydrogen peroxide (H_2O_2), which led to reduced cell viability.

2. Results and Discussion

2.1. Surface Coating-Dependent Interaction of Nanoparticles with Endothelial Cells and Macrophages

Successful artificial organelles need to fulfil a lot of different requirements including their assembly and testing in buffer solution followed by their internalization by cell with preserved structural integrity and function. The first aspect we considered was the uptake efficiency of core–shell particles depending on the outermost surface coating to ensure high internalization. Herein, we chose 800 nm core–shell particles due to their desirable high loading of enzyme-loaded liposomes with preserved colloidal stability and possibility for surface modification. Admittedly, the particles might be fast filtered out by the organs when administered in vivo due to their size and hardness, yet these particles are still able to illustrate the potential of subcompartmentalized artificial organelles.

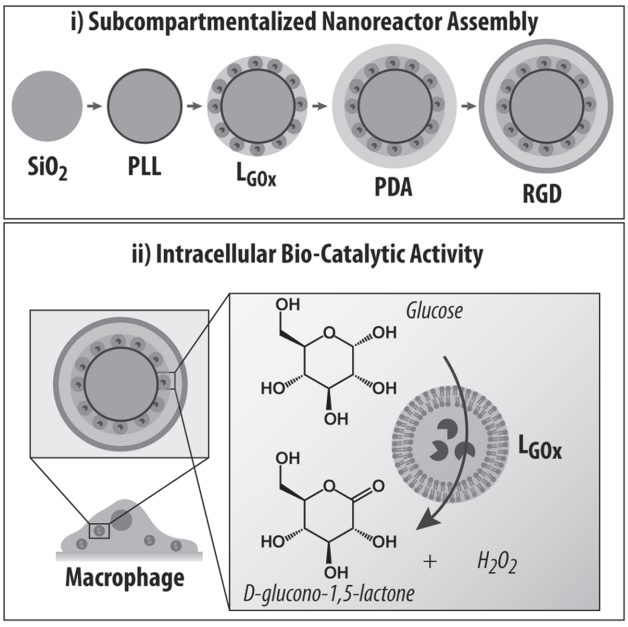

Scheme 1. Schematic illustration of i) the assembly of the subcompartmentalized nanoreactors starting with PLL coating of silica particles followed by the deposition of L_{GOx}, PDA, and RGD, and ii) the intracellularly active subcompartmentalized nanoreactors with encapsulated glucose oxidase in the liposomal subunits (L_{GOx}) including the illustration of the enzymatic conversion of glucose into D-glucono-1,5-lactone and H_2O_2.

2.1.1. Coating

First, the particles were coated with a layer of fluorescein isothiocyanate labeled poly(L-lysine) (PLL_F) to visualize the particles when internalized by the cells. Next, a thin layer of PDA was adsorbed. PDA, deposited by the self-polymerization of dopamine (DA) at slightly basic pH, is an interesting material to be used for various biomedical applications as recently extensively reviewed by us[15] and others.[16] Among the many advantages is the opportunity for postmodification with amines and thiols. We employed the graft copolymer PLL-*graft* -PEG with unmodified or RGD end-functionalized PEG chains, a copolymer with prior success in biomedicine, for instance, as surface coating,[17] for biolubrication,[18] or for DNA delivery.[19] This polymer layer equipped the particles with cell-adhesive (RGD) or cell-repellent (PEG) properties, since the amine groups on the PLL allowed for the

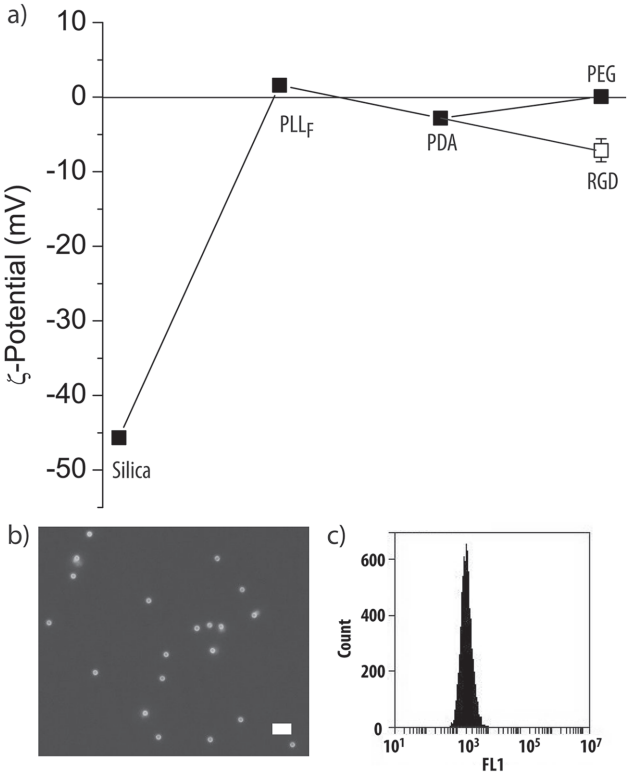

Figure 1. a) ζ-Potential of the SiO_2 particles measured after the different coating steps in HEPES[1] buffer. b) Representative fluorescent microscopy image of P^{RGD}. The scale bar is 2 µm. c) Flow cytometry histogram of P^{RGD}. Experiments in (b) and (c) were performed in HEPES[2] buffer.

interaction with the quinons of the PDA. The particles will be labeled P^{PDA}, P^{PEG}, and P^{RGD} from now on.

The deposition of these polymer layers was confirmed by measuring the ζ-potential of the particles (**Figure 1**a). The initial negative ζ-potential of the silica particles in 10×10^{-3} M 4-(2-hydroxyethyl)piperazine-1-ethanesulfonic acid (HEPES) buffer (pH 7.4, HEPES[1] buffer) increased upon the deposition of PLL_F, followed by a slight drop when the PDA layer was adsorbed. P^{PEG} and P^{RGD} had a ζ-potential of ≈0 and ≈ –10 mV, respectively. This observation together with our prior report on the deposition of PLL-*g*-PEG onto PDA[20] suggested the successful deposition of the final polymer layer. P^{RGD} was visualized in buffer solution (HEPES[2] buffer: 10×10^{-3} M HEPES and 150×10^{-3} M NaCl (pH 7.4)) as a representative example using an epifluorescent microscope (Figure 1b). The homogenous fluorescence, due to the presence of PLL_F, confirmed that the PDA layer was thin enough to not entirely block the fluorescence emission. This aspect was important since we have prior observed that thick layers of PDA could entirely hinder the visualization of fluorescently labeled underlying layers.[11] Furthermore, the particles remained well dispersed without aggregation, which was also supported when considering the flow cytometry histogram using particles suspended in HEPES[2] buffer (Figure 1c). The nonaggregated state of the particles was important to ensure that differences in the biological evaluation were only due to varied surface chemistries and not due to changes in size, i.e., aggregates versus individual particles.

2.1.2. Uptake by Endothelial Cells and Macrophages

Intracellularly active nanoreactors need to fulfil multiple requirements including the internalization by the targeted cell line. Therefore, we aimed at comparing the uptake of P^{PDA}, P^{PEG}, and P^{RGD} by macrophages and endothelial cells in static conditions and with applied shear stress. These two cell types were chosen because they are interesting targets for artificial organelles and are straight forward accessible upon intravenous injection. Macrophages are the body's first line of defense against intruding pathogens. However, microorganisms have come up with ways to avoid or escape the digestive organelles of immune cells leading to severe medical conditions. For instance, adherent-invasive *Escherichia coli* bacteria can resist macrophage degradation in Crohn's disease patients,[21] or *Mycobacterium tuberculosis* is a microorganism that has adapted to survive in macrophage phagosomes.[22] Since traditional treatment strategies did not succeed, novel concepts such as TCM are required, i.e., equipping macrophages with artificial digestive reactors might present itself as an alternative approach to battle resistant invaders.

Static Conditions: The first step for an artificial organelle to support its host cell is to be internalized. With the aim to compare the uptake of P^{PDA}, P^{PEG}, and P^{RGD} by endothelial cells and macrophages, 6250 and 2500 particles mL^{-1} were incubated with endothelial cells and macrophages, respectively, at static conditions (τ_0 = 0 dyn cm^{-2}). Different particle concentrations were used to keep the particles to cell ratio constant at 10/1. The normalized cell mean fluorescence (nCMF; **Figure 2**) was assessed at different time points using flow cytometry. Endothelial cells exhibited similar nCMF independent on the used particles. Unexpectedly, the endothelial cells did not show any preference to P^{RGD} (Figure 2a). Furthermore, the nCMF was highest after 2 h, followed by a constant decrease over the subsequent 21 h. On the other hand, macrophages showed constant nCMF between 3 and 24 h exposure times to the particles (Figure 2b). Additionally, P^{RGD} led to the expected significantly higher nCMF compared to P^{PDA} and P^{PEG} for all tested time points.

Applied Shear Stress: Assessing the interaction of drug carriers and cells, using predominantly endothelial cells, with applied shear stress starts to be recognized as an important factor as recently reviewed by Godoy-Gallardo et al.[23] Endothelial cells line our blood vessel and are therefore permanently exposed to blood flow. Furthermore, circulating macrophages experience the same mechanical forces, and its relevance has recently been reported by us[24] and others.[25] Since every potential artificial organelle administered intravenously will be exposed to the blood stream and the induced mechanical forces such as shear stress, the uptake of P^{PDA}, P^{PEG}, and P^{RGD} by endothelial cells, and macrophages were reassessed with applied shear stress (τ_4 = 4 dyn cm^{-2}) using a commercial microfluidic setup. The nCMF of the cells upon exposure to the different particles was monitored after 2 h for macrophages and 16 h for endothelial cells and compared to the nCMF obtained at τ_0 (**Figure 3**). For endothelial cells, the nCMF due to the exposure of the cells to P^{RGD} was

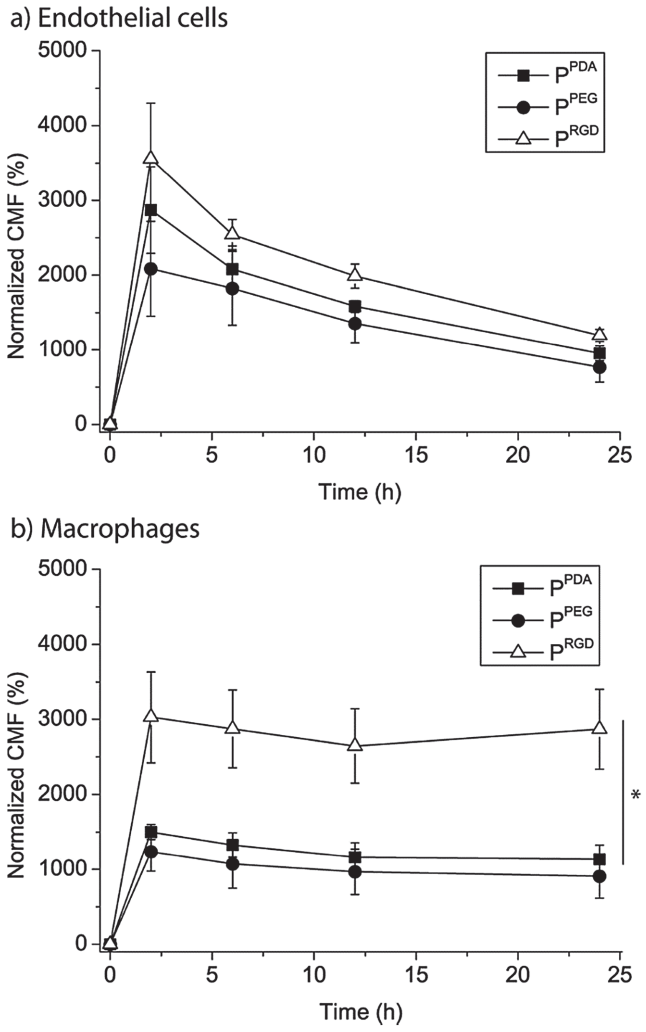

Figure 2. The normalized CMF of a) endothelial cells and b) macrophages exposed to P^{PDA}, P^{PEG}, and P^{RGD} depending on the incubation time is shown ($n = 3$, $^{*}p < 0.05$).

significantly higher compared to P^{PDA} and P^{PEG} at τ_4, while the nonsignificant difference at τ_0 was confirmed. For macrophages, the nCMF due to the exposure of the cells to P^{RGD} was significantly higher compared to P^{PDA} and P^{PEG} at τ_0 and τ_4. Furthermore, the nCMF of both cell types exposed to P^{RGD} was significantly higher at τ_4 compared to τ_0, while no significant difference was observed for P^{PDA} and P^{PEG}.

With the aim to confirm the uptake of the particles by the cells, endothelial cells and macrophages exposed to P^{RGD} with applied shear stress (τ_4) for 16 and 2 h, respectively, were fixed, stained, and visualized by confocal laser scanning microscopy (CLSM). The endothelial cells had only very few internalized particles (**Figure 4**, right). On the other hand, macrophages had a high amount of internalized particles (Figure 4, left). The visualization confirmed the flow cytometry results. Due to the size and mechanical properties of the particles, the results were expected. Immune cells are known to be able to internalize much larger particles than other type of cells without the activation of a specific endocytotic pathway such as the intercellular adhesion molecule 1 mediated uptake.[26] Furthermore, we would like to note

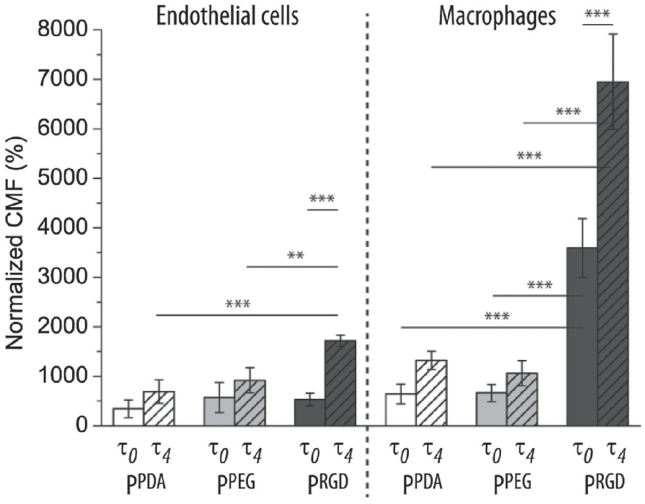

Figure 3. Normalized CMF of endothelial cells and macrophages upon exposure to P^{PDA}, P^{PEG}, or P^{RGD} for 16 and 2 h, respectively, with applied shear stress (τ_4) compared to the static condition (τ_0) ($n = 4$, $^{**}p < 0.01$, $^{***}p < 0.001$).

that there were many noninternalized particles observed when using endothelial cells, while this was not the case for samples with macrophages. Employing the CLSM images and flow cytometry results, we estimated the number of internalized particles for the macrophages to be ≈37 and ≈74 at τ_0 and τ_4, respectively.

Following on, we assessed the cell viability of endothelial cells and macrophages with applied shear stress τ_4 when exposed to P^{RGD} in comparison to τ_0 after 16 and 2 h, respectively (**Figure 5**). The cell viability was normalized to cells only at τ_0. First, exposure to P^{RGD} did not negatively affect the cells for τ_0 and τ_4. Interestingly, a ≈60% higher number of viable endothelial cells were detected at τ_4. The appearance of the cells depending on the applied shear stress and the presence of P^{RGD} was visualized using bright field microscopy (**Figure 6**). More endothelial cells were observed at τ_4 in agreement with the quantitative cell viability results. Since this type of cells is permanently exposed to the blood flow and the induced mechanical forces, it is not surprising that conditions which mimic the biological environment have beneficial effect on the endothelial cells. Furthermore, the number of macrophages was similar but they were found to have a more rounded morphology at τ_4. We have prior found

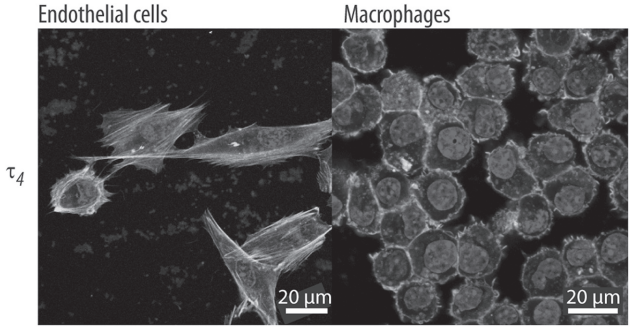

Figure 4. CLSM images of endothelial cells and macrophages exposed to P^{RGD} with applied shear stress (τ_4) for 16 and 2 h, respectively.

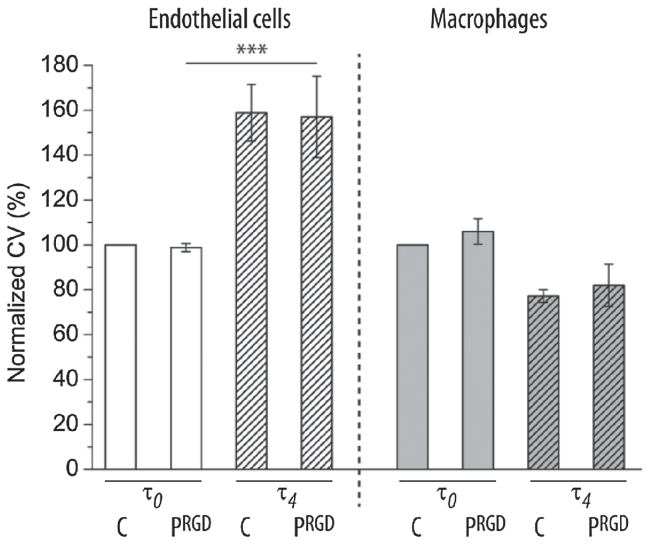

Figure 5. Normalized cell viability of endothelial cells and macrophages upon exposure to P^{RGD} in comparison to cell only (C) at τ_0 and τ_4 for 16 and 2 h, respectively, ($n = 3$, $^{***}p < 0.001$).

that shear stress affected the number of macrophages likely due to their semiadherent nature.[24b]

2.2. Nanoreactor

Following on, we aimed at assembling enzyme-loaded subcompartmentalized nanoreactors and to test such a system for the first time toward its intracellular activity. Glucose oxidase was chosen as enzyme since it converts glucose into H_2O_2, a cytotoxic compound. This aspect provides a straight-forward method to monitor the intracellular activity of the nanoreactors by assessing the viability of the macrophages.

2.2.1. Assembly

Inspired by our prior work,[27] we deposited glucose oxidase-loaded 1,2-ditetradecanoyl-*sn*-glycero-3-phosphocholine/1,2-dihexadecanoyl-*sn*-glycero-3-phosphocholine liposomes (L_{GOx}) as subunits on 800 nm PLL precoated silica particles followed by the deposition of PDA overnight and PLL-*g*-PEG/RGD ($P^{RGD}{}_{LGOx}$). As we have previously shown, PLL allows for the immobilization of different types of liposomes without their rupturing,[11] and the subsequent PDA deposition did not lead to their rupturing or displacement.[27] CLSM was employed to confirm that the assembly of the nanoreactors was successful. In this context, fluorescently labeled GOx (GOx_{633}) was incorporated into NBD-labeled liposomes (L_{NBD}). **Figure 7**ai,ii shows that the nanoreactors were homogenously coated with both L_{NBD} and GOx_{633}. As control, the PLL precoated silica particles were exposed to a solution of GOx_D followed by coating with PDA and PLL-*g*-PEG/RGD ($P^{RGD}{}_{GOx}$) with the aim to demonstrate that the activity comes from enzymes within the liposomal subunits only. (GOx_D refers to GOx treated the same way as for encapsulation into liposomes but without using lipids.) The time-dependent conversion of 100×10^{-3} M glucose into H_2O_2 by 100 reactors μL^{-1} was monitored using the Amplex Red assay and reading out of the fluorescent intensity ($\lambda = 598$ nm) using a multimode plate reader (Figure 7b). As expected, only the sample containing nanoreactors with GOx encapsulated within the liposomal subunits exhibited increasing fluorescent intensities, i.e., only $P^{RGD}{}_{LGOx}$ was able to convert glucose into H_2O_2. On the other hand, $P^{RGD}{}_{GOx}$ showed

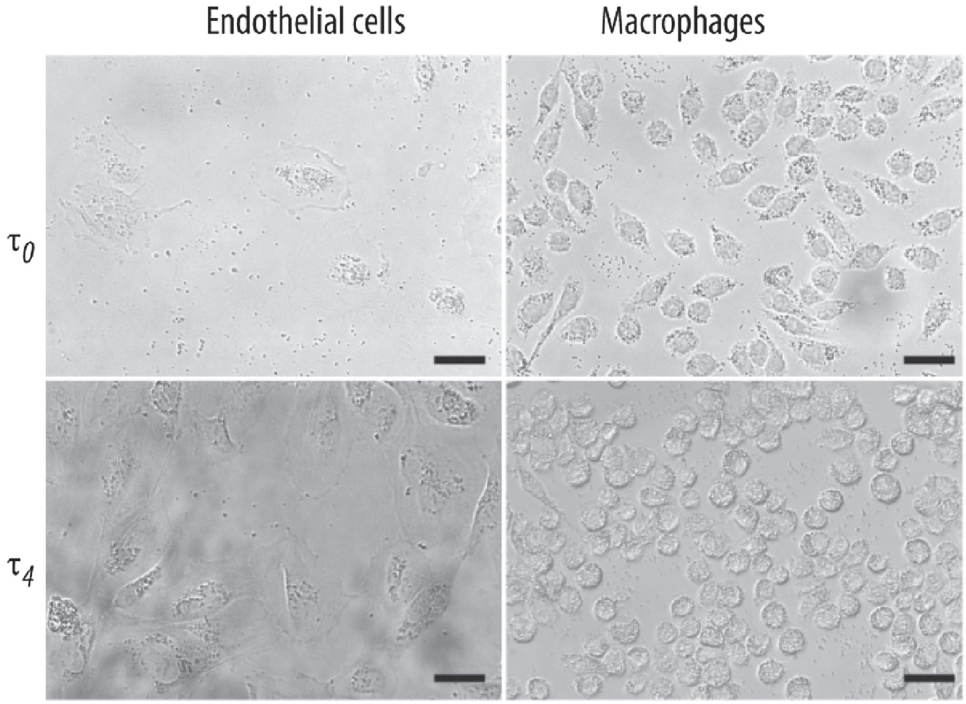

Figure 6. Representative bright field images of endothelial cells and macrophages upon exposure to P^{RGD} at τ_0 and τ_4 for 16 and 2 h, respectively.

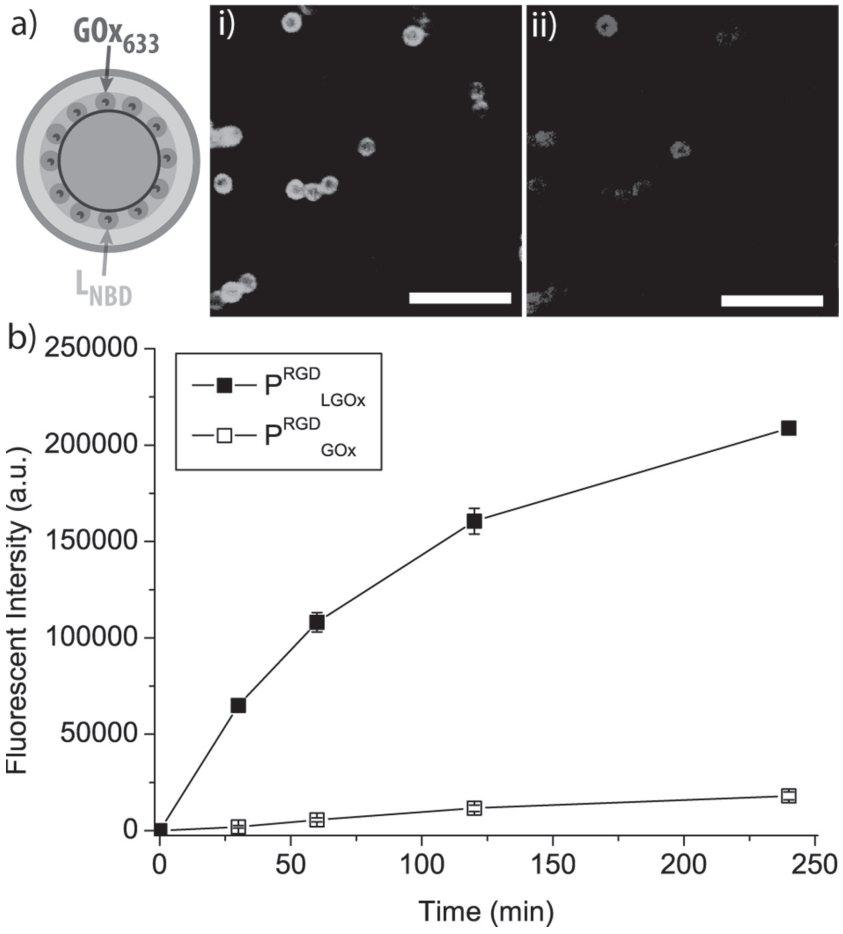

Figure 7. a) CLSM images of nanoreactors coated with i) fluorescently labeled liposomes (L_{NBD}) and ii) fluorescently labeled GOx (GOx_{633}). b) Nanoreactor activity: The time-dependent conversion of glucose into H_2O_2 by $P^{RGD}{}_{LGOx}$ and $P^{RGD}{}_{GOx}$ is shown.

very low fluorescent intensity strongly suggesting the absence or denaturation of GOx in the assembly. Furthermore, employing the calibration curve for GOx (Figure S1, Supporting Information) and assuming that 1 U corresponds to the production of 1 μmol H_2O_2 per min, the amount of produced H_2O_2 per nanoreactor was estimated on the basis of the recorded FI after 30 min (Figure 7) and a concentration of 100 nanoreactors μL^{-1}. Accordingly, the estimated H_2O_2 production rate per nanoreactor was $\approx 3 \times 10^{-9}$ μmol min^{-1}.

2.2.2. Intracellular Activity

With the aim to demonstrate that the assembled nanoreactors exhibited intracellular activity, they were employed to kill the host cells using the produced H_2O_2 to illustrate the function of the potential artificial organelles to counteract pathogenic invasion in macrophages. First, the dose response curve for macrophages exposed to glucose was measured (Figure S2, Supporting Information). 100×10^{-3} M glucose was chosen as a concentration which did not negatively affect the cells, but enough H_2O_2 should be produced to monitor the reduction in cell viability and by doing so, the intracellular activity of the nanoreactors was confirmed. In an attempt to visualize both components of the subcompartmentalized reactor inside of the macrophages using CLSM, $P^{RGD}{}_{LGOx}$ was assembled using L_{NBD} and GOx_{633}. We would like to note that the PDA coating in this case was much thinner (only 15 min PDA coating) in order to be able to detect the fluorescence by CLSM. This thinner PDA coating was likely to affect the stability of the nanoreactors inside of the cells and therefore, we chose 6 h incubation time. Although both, L_{NBD} and GOx_{633} were observed, only a few colocalized spots could be identified (Figure S3, Supporting Information). We attributed this aspect to the fact that lipids coated with a PDA capping layer could be internalized by cells in a PDA coating thickness depending manner as we have previously shown.[28] On the other hand, increasing the thickness of the PDA layer hindered the fluorescent imaging as we have previously reported.[11] As a consequence, CLSM images of the fluorescently labeled nanoreactors inside the macrophages yielded poor quality images.

Following on, the subcompartmentalized reactor $P^{RGD}{}_{LGOx}$ was incubated with macrophages for 2 h followed by two washing steps with PBS and incubation with 100×10^{-3} M glucose for 6 and 24 h. We would like to note that the PDA coating time of these nanoreactors was sufficiently long to ensure that the PDA thickness was sufficiently high to avoid the above-mentioned issue for the chosen time points. As controls, the macrophages were exposed to $P^{RGD}{}_{LGOx}$ without the addition of glucose, macrophages were only incubated with glucose but not with $P^{RGD}{}_{LGOx}$, or the cells remained entirely untreated. The washing step was important to ensure that the reactors which were not internalized were removed. The success of this step has been confirmed by CLSM in Figure 4. The viability of the cells was assessed and compared. The absorbance readings, representing the not normalized cell viability, showed significant lower viability when the macrophages were exposed to both $P^{RGD}{}_{LGOx}$ and glucose after 6 and 24 h compared to the untreated cells (**Figure 8**a). Importantly, there was no significant difference in the absorbance reading between the untreated cells and the cells exposed to either $P^{RGD}{}_{LGOx}$ or glucose only after 6 and 24 h. Furthermore, when normalizing the raw data to the untreated cells, the viability of cells exposed to $P^{RGD}{}_{LGOx}$ and glucose after 6 and 24 h was significantly lower compared to the controls (Figure 8b). Additionally, the normalized viability of the macrophages incubated with $P^{RGD}{}_{LGOx}$ and glucose for 6 h was significantly higher compared to an incubation time of 24 h. These results strongly suggest that H_2O_2 was produced by the subcompartmentalized reactor intracellularly leading to cell death. Considering the assumption that one nanoreactor produces $\approx 3 \times 10^{-9}$ μmol min^{-1} H_2O_2 and that all the 37 nanoreactors

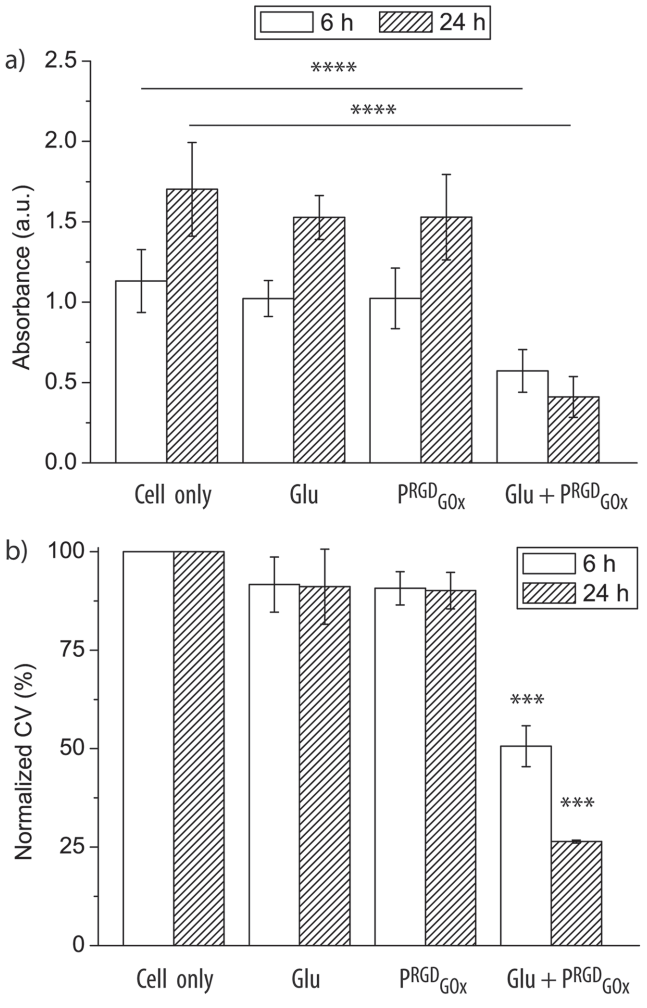

Figure 8. Intracellular active subcompartmentalized nanoreactor: a) normalized cell viability of macrophages b) exposed to Glu, $P^{RGD}{}_{LGOx}$ or Glu, and $P^{RGD}{}_{LGOx}$ compared to cell only after 6 and 24 h (n = 3, $^{***}p < 0.001$, $^{****}p < 0.0001$).

per cell were functional and no H_2O_2 was degraded by inherent cellular activity, 0.04 nmol H_2O_2 was produced within one macrophage after 6 h leading to the observed reduction in viability. Furthermore, employing the dose response curve of macrophages exposed to H_2O_2 (Figure S4, Supporting Information), we estimated that the cell viability was reduced to a similar amount as when the macrophages were exposed to media containing $\approx 1.4 \times 10^{-3}$ M H_2O_2.

3. Conclusion

In summary, we assembled the first subcompartmentalized nanoreactor with intracellular activity. The uptake efficiency was found to be dependent on the surface coating and the presence of shear stress, with significant higher internalization for RGD-modified particles with applied shear stress for endothelial cells and macrophages. The loading of GOx into the liposomal subunit of the nanoreactor was confirmed and the activity was demonstrated by the conversion of glucose. Finally, macrophages with internalized $P^{RGD}{}_{LGOx}$ exhibited reduced cell viability upon exposure to glucose compared to the controls, demonstrating the intracellular function of the nanoreactors. These results provide a considerable contribution to the field of TCM by assembling nanoreactors, which could act as artificial organelles.

4. Experimental Section

Materials: Sodium chloride (NaCl), poly(L-lysine) hydrobromide (PLL, 40–60 kDa), phosphate buffered saline (PBS), 4-(2-hydroxyethyl)piperazine-1-ethane-sulfonic acid (HEPES), chloroform anhydrous (≥99%), dimethyl sulfoxide (DMSO), glucose oxidase from *Aspergillus niger* (GOx, ≥15 units mg^{-1} solid, 160 kDa), catalase from bovine liver (10 000 units mg^{-1} solid, 240 kDa), peroxidase from horseradish (HRP, 250–330 units mg^{-1} solid), paraformaldehyde (PFA), tris(hydroxymethyl)-aminomethane (TRIS), dopamine hydrochloride, 4′,6-diamidino-2-phenylindole dihydrochloride (DAPI), phalloidin-tetramethylrhodamine B isothiocyanate (phalloidin-TRITC), cell counting kit-8 (CCK-8), *o*-dianisidine, polyethylene glycol-*tert*-octylphenyl ether (Triton X-100), D-glucose (≥99.5%), and hydrogen peroxide (H_2O_2, 30% w/w) were purchased from Sigma-Aldrich.

Zwitterionic lipids, 1,2-ditetradecanoyl-*sn*-glycero-3-phosphocholine (DMPC, T_m = 23 °C), 1,2-dihexadecanoyl-*sn*-glycero-3-phosphocholine (DPPC, T_m = 41 °C), and 1-myristoyl-2-[12-[(7-nitro-2-1,3-benzoxadiazol-4-yl)amino]dodecanoyl]-*sn*-glycero-3-phosphocholine (NBD) were purchased from Avanti Polar Lipids (Alabama, USA). Silica particles (0.8 µm in diameter) were obtained from Microparticles GmbH (Berlin, Germany). Amplex Red Glucose/Glucose Oxidase Assay Kit and Alexa Flour 633 C5 maleimide (AF633) reactive dye were purchased from Life Technologies (Carlsbad, USA).

Poly(L-lysine (20 kDa))-*graft* [3.5]-poly(ethylene glycol (2 kDa)) (PLL-*g*-PEG) and poly(L-lysine (20 kDa))-*graft* [3.5]-poly(ethylene glycol (2 kDa)/poly(ethylene glycol (2 kDa))/L-arginine-glycine-L-aspartic acid (RGD)) (PLL-*g*-PEG/RGD) (6–15% of PEG (3.4 kDa) is functionalized with RGD) were obtained from SoSuS AG (Dübendorf, Switzerland).

Three buffers were used: (i) HEPES[1] buffer consisting of 10×10^{-3} M HEPES (pH 7.4), (ii) HEPES[2] buffer consisting of 10×10^{-3} M HEPES and 150×10^{-3} M NaCl (pH 7.4), and (iii) TRIS buffer consisting of 10×10^{-3} M TRIS (pH 8.5). All buffers were made using ultrapure water (Milli-Q gradient A 10 system, resistance 10 MΩ cm, TOC <4 ppb, Millipore Corporation, USA).

Unilamellar liposomes were prepared by evaporation of 100 µL chloroform/lipid solution (25 mg mL^{-1} DMPC:DPPC 84:16 wt%) under vacuum for at least 1 h, followed by rehydration of the lipids in 200 µL HEPES[2] containing 5 mg mL^{-1} GOx (L_{GOx}). L_{GOx} was then further hydrated with 800 µL HEPES[2]. The solutions were extruded through 100 nm filters (11×) to obtain monodisperse liposomes. Nonencapsulated enzymes were removed by dialyzing the sample for 2 h under stirring against HEPES[2] (MWCO 100 kDa membranes). The liposome formation was confirmed by analyzing the solutions by dynamic light scattering (DLS, Zetasizer Nano S90) using a material refractive index of 1.590 and a dispersant (water at 25 °C) refractive index of 1.330.

Core–Shell Particles of Cell Uptake Experiments: 200 µL (50 mg mL^{-1}) of 0.8 µm diameter silica particles was washed 2× in HEPES[2] buffer, coated with PLL_{FITC} (1 mg mL^{-1}, 15 min), and washed 3× in TRIS buffer. All washing steps were performed in a bench top

centrifuge (MiniSpin, Eppendorf) at 1500 rpm for 3 min. Next, the particles were exposed to a dopamine (DA) solution (2 mg mL^{-1}, 15 min), followed by 3× washing in HEPES[2] buffer yielding P^{PDA} particles. If needed, these particles were further coated by incubation in either a PLL-*g*-PEG (1 mg mL^{-1} in HEPES[2] buffer, 30 min) or a PLL-*g*-PEG/RGD (1 mg mL^{-1} in HEPES[2] buffer, 30 min) solution, followed by 3× washing in HEPES[2] buffer to obtain P^{PEG} and P^{RGD}, respectively. The ζ-potential of the particles was analyzed by dispersing 1 µL of the final particles in 999 µL HEPES[1] buffer. The analysis was carried out at each deposition step using a Zetasizer Nano ZS (Malvern Instruments).

The fluorescence and concentration of all particles was measured by flow cytometry prior to the cell experiments.

Nanoreactor Assembly: 200 µL (50 mg mL^{-1}) of 0.8 µm silica particles was washed 2× in HEPES[2] buffer, coated with PLL (1 mg mL^{-1} in HEPES[2] buffer, 15 min), followed by 3× washing in HEPES[2] buffer. Then, the particles were exposed to an L_{GOx}, stock solution for 30 min followed by 3× washing in HEPES[2] buffer. The particles were then washed 3× in TRIS buffer and incubated with in a DA solution (2 mg mL^{-1} in TRIS buffer) overnight, followed by 3× washing in HEPES[2] buffer. Finally, the particles were coated with PLL-*g*-PEG/RGD (1 mg mL^{-1} in HEPES[2] buffer, 30 min) and washed 3× washing in HEPES[2] buffer. Fluorescently labeled P^{RGD}_{LGOx} was assembled by using liposomes NBD lipids (2.5 mg mL^{-1}), AF633-labeled GOx, and the PDA was allowed to deposit for 15 min.

Nanoreactor Activity: The assembled nanoreactors were counted using flow cytometry. 50 µL of the particle samples (100 particles μL^{-1}) was incubated in a 96-well plate at 37 °C with 100×10^{-3} M glucose at different time points. After incubation, 50 µL of a working solution consisting of 100×10^{-6} M Amplex Red (Life Science) and 0.2 U mL^{-1} horse radish peroxidase in HEPES[2] was added to each well, and the fluorescence ($\lambda = 598$ nm) was immediately measured using a multimode plate reader.

Cell Work: RAW 264.7 mouse macrophage and human umbilical vein endothelium cells (HUVEC) cell lines were purchased from European Collection of Cell Cultures. The macrophages were cultured in 75 cm^2 culture flasks (1 100 000 cells per flask in 20 mL medium) at 37 °C and 5% CO_2 using Dulbecco's modified Eagle's medium (DMEM, with 4500 mg mL^{-1} glucose, sodium pyruvate, and sodium bicarbonate) and added 10% fetal bovine serum (FBS), penicillin (50 µg mL^{-1}), and streptomycin (50 µg mL^{-1}). The endothelial cells were cultured in 75 cm^2 culture flasks (250 000 cells per flask in 20 mL medium) at 37 °C and 5% CO_2 using Medium 200 (Invitrogen) supplemented with 50 µg mL^{-1} penicillin, 50 µg mL^{-1} streptomycin, and 2% large vessel endothelial supplement (Invitrogen).

At least 2000 cells were analyzed and at least three independent repeats were performed for all the reported flow cytometry analysis (C6 Flow Cytometer, Accuri Cytometer, Inc.) using an excitation wavelength of 488 nm. The autofluorescence of the cells was subtracted by analyzing control samples where no particles were added. All data were normalized to the fluorescence of the particles which were measured using a multimode plate reader. Unless otherwise noted, the statistical significance used to compare the distribution was determined using a one-way ANOVA with a confidence level of 95% ($\alpha = 0.05$), followed by a Tukey's multiple comparison posthoc test ($^*p < 0.05$).

Uptake Experiments—Static Conditions: Macrophages (50 000 cells per well) and endothelial cells (20 000 cells per well) were seeded in a 96-well plate. Each well was washed 2× in PBS and 100 µL P^{PDA}, P^{PEG}, or P^{RGD} suspended in the corresponding media was added (particle/cells 10:1). The cells and particles were incubated at 37 °C in 5% CO_2 for 2, 6, 12, and 24 h. Then, each well was washed 2× in PBS and the cells were harvested for analysis by flow cytometry.

Uptake Experiments—Dynamic Conditions: The ibidi Pump System (ibidi GmbH, Munich, Germany) was employed to apply controlled shear stress. Macrophages (100 000 cells per channel) and endothelial cells (40 000 cells per channel) were seeded in closed perfusion channels (µ-slide VI 0.4 six-well ibiTreat channels) and allowed to attach at 37 °C in 5% CO_2 for 16 and 4 h, respectively. Afterwards, 7.5 mL of corresponding media containing P^{PDA}, P^{PEG}, or P^{RGD} (particle/cell 10:1) was added to the syringes of the pump system, which were connected to the channels, and a shear stress ($\tau_4 = 4$ dyn cm^{-2}) was applied for 2 and 16 h for macrophages and endothelial cells, respectively, at 37 °C in 5% CO_2. As a control, 120 µL of medium with no shear stress ($\tau_0 = 0$ dyn cm^{-2}) and no particles was employed. The channels were washed 2× with 120 µL PBS, and the cells were harvested for analysis by flow cytometry.

Cell Viability: The viability of the cells was assessed after exposure to P^{RGD} as described above using dynamic conditions. Following on, the channels were washed 2× with the corresponding media and 110 µL media and 10 µL of CCK-8 (Dojindo) solution was added to each channel. The cells were incubated for 2 h at 37 °C in 5% CO_2. Then, 100 µL of the solution from each channel was transferred to a 96-well plate and analyzed using a multimode plate reader by measuring the absorbance at 450 nm. Three independent repeats were performed and the results were normalized to cells in the absence of P^{RGD} at τ_0.

Intracellular Nanoreactor Activity: Macrophages were seeded in 96 well plates (50 000 cells per well) and allowed to attach overnight at 37 °C in 5% CO_2. The cells were then washed 2× with 100 µL PBS, incubated with P^{RGD}_{LGOx} (particles/cells 10:1) for 2 h at 37 °C in 5% CO_2, and washed 2× with PBS before adding media with 100×10^{-3} M glucose or without added glucose for 6 or 24 h. As controls, cells without exposure to P^{RGD}_{LGOx} were considered. The cells were washed 2× in PBS and 110 µL cell medium containing 10 µL of CCK-8 solution was added to each well and incubated for 2 h at 37 °C in 5% CO_2. Finally, 100 µL of the solution from each well was transferred to a 96-well plate and analyzed using a multimode plate reader (absorbance at 450 nm). Three independent repeats were conducted. The statistical significance used to compare the distribution was determined using a two-way ANOVA with a confidence level of 95% ($\alpha = 0.05$), followed by a Tukey's multiple comparison posthoc test ($^*p < 0.05$).

Glucose Dose Response: Macrophages were seeded in a 96-well plate (50 000 cells per well) and allowed to attach overnight at 37 °C in 5% CO_2. The cells were then washed 2× with 100 µL PBS and incubated with different concentrations of glucose for 6 or 24 h. The cells were washed 2× in PBS and 110 µL cell medium containing 10 µL of CCK-8 solution was added to each well and incubated for 2 h at 37 °C in 5% CO_2. Finally, 100 µL of the solution from each well was transferred to a 96-well plate and analyzed using a multimode plate reader (absorbance at 450 nm). Three independent repeats were performed.

Imaging: Macrophages (100 000 cells per channel) were seeded in closed perfusion channels (µ-slide VI 0.4 six-well

ibiTreat channels) and allowed to attach at 37 °C in 5% CO_2 overnight. The cells were then washed 2× with PBS and incubated with fluorescently labelled P^{RGD}_{LGOx} for 6 h in a particle to cell ratio of 10/1. After incubation, the cells were washed twice with 100 µL PBS; 100 µL PFA (4%) was added to each channel, washed twice with 100 µL PBS and washed once with 100 µL of 0.1% Triton-X in PBS (T-PBS). 100 µL DAPI (1 µg mL^{-1} in PBS) was added to each channel and incubated for 30 min at room temperature in aluminum foil. The channel was then washed thrice in T-PBS and finally 100 µL PBS was added for storage. Confocal laser scanning fluorescence microscopy was conducted using a Zeiss Axiovert microscope coupled to a LSM 700 confocal scanning module (Carl Zeiss, Germany) and a 100× oil-immersion objective.

Supporting Information

Supporting Information is available from the Wiley Online Library or from the author.

Acknowledgements

This project was supported by a grant from the Danish Research Council for Independent Research-Technology and Production (DFF-FTP).

[1] A. Dillin, D. E. Gottschling, T. Nyström, *Curr. Opin. Cell Biol.* **2014**, *26*, 107.
[2] A. Jurecka, A. Tylki-Szymanska, *Expert Opin. Orphan Drugs* **2015**, *3*, 293.
[3] a) R. Peters, I. Louzao, J. C. M. van Hest, *Chem. Sci.* **2012**, *3*, 335; b) P. Tanner, P. Baumann, R. Enea, O. Onaca, C. Palivan, W. Meier, *Acc. Chem. Res.* **2011**, *44*, 1039.
[4] N. Ben-Haim, P. Broz, S. Marsch, W. Meier, P. Hunziker, *Nano Lett.* **2008**, *8*, 1368.
[5] S. F. M. van Dongen, W. P. R. Verdurmen, R. J. R. W. Peters, R. J. M. Nolte, R. Brock, J. C. M. van Hest, *Angew. Chem., Int. Ed.* **2010**, *49*, 7213.
[6] P. Tanner, O. Onaca, V. Balasubramanian, W. Meier, C. G. Palivan, *Chemistry – A Eur. J.* **2011**, *17*, 4552.
[7] F.-P. Chang, Y. Hung, J.-H. Chang, C.-H. Lin, C.-Y. Mou, *ACS Appl. Mater. Interfaces* **2014**, *6*, 6883.
[8] a) L. Hosta-Rigau, B. Stadler, in *Regenerative Medicine, Artificial Cells and Nanomedicine: Selected Topics in Nanomedicine*, Vol. *3* (Ed: T. M. S. Chang), World Science Publisher/Imperial College Press, Singapore, **2013**; b) M. Marguet, C. Bonduelle, S. Lecommandoux, *Chem. Soc. Rev.* **2013**, *42*, 512.
[9] R. Chandrawati, F. Caruso, *Langmuir* **2012**, *28*, 13798.
[10] R. J. R. W. Peters, M. Marguet, S. Marais, M. W. Fraaije, J. C. M. van Hest, S. Lecommandoux, *Angew. Chem., Int. Ed.* **2014**, *53*, 146.
[11] L. Hosta-Rigau, M. J. York-Duran, Y. Zhang, K. N. Goldie, B. Städler, *ACS Appl. Mater. Interfaces* **2014**, *6*, 12771.
[12] P. Schattling, C. Dreier, B. Stadler, *Soft Matter* **2015**, *11*, 5327.
[13] L. Hosta-Rigau, M. J. York-Duran, T. S. Kang, B. Stadler, *Adv. Funct. Mater.* **2015**, *25*, 3860.
[14] R. Chandrawati, S.-F. Chong, A. N. Zelikin, L. Hosta-Rigau, B. Stadler, F. Caruso, *Soft Matter* **2011**, *7*, 9638.
[15] M. E. Lynge, P. Schattling, B. Städler, *Nanomedicine* **2015**, *10*, 2725.
[16] Y. Liu, K. Ai, L. Lu, *Chem. Rev.* **2014**, *114*, 5057.
[17] a) B. Stadler, D. Falconnet, I. Pfeiffer, F. Hook, J. Voros, *Langmuir* **2004**, *20*, 11348; b) J. W. Lussi, D. Falconnet, J. A. Hubbell, M. Textor, G. Csucs, *Biomaterials* **2006**, *27*, 2534; c) R. Ogaki, M. Foss, *Langmuir* **2014**, *30*, 7014; d) S. G. Ricoult, G. Thompson-Steckel, J. P. Correia, T. E. Kennedy, D. Juncker, *Biomaterials* **2014**, *35*, 727.
[18] A. Dedinaite, *Soft Matter* **2012**, *8*, 273.
[19] T. Luehmann, M. Rimann, A. G. Bitterman, H. Hall, *Bioconj. Chem.* **2008**, *19*, 1907.
[20] B. M. Teo, R. van der Westen, L. Hosta-Rigau, B. Städler, *BBA-Gen. Subjects* **2013**, *1830*, 4838.
[21] M.-A. Bringer, A.-L. Glasser, C.-H. Tung, S. Méresse, A. Darfeuille-Michaud, *Cell. Microbiol.* **2006**, *8*, 471.
[22] D. Schnappinger, S. Ehrt, M. I. Voskuil, Y. Liu, J. A. Mangan, I. M. Monahan, G. Dolganov, B. Efron, P. D. Butcher, C. Nathan, G. K. Schoolnik, *J. Exp. Med.* **2003**, *198*, 693.
[23] M. Godoy-Gallardo, P. K. Ek, M. M. T. Jansman, B. M. Wohl, L. Hosta-Rigau, *Biomicrofluidics* **2015**, *9*, 052605.
[24] a) K. Panneerselvam, M. E. Lynge, C. F. Riber, S. Mena-Hernando, A. A. A. Smith, K. N. Goldie, A. N. Zelikin, B. Städler, *Biomicrofluidics* **2015**, *9*, 052610; b) K. Panneerselvam, S. Mena-Hernando, B. M. Teo, K. N. Goldie, B. Stadler, *RSC Adv.* **2014**, *4*, 44769.
[25] a) L. Castro-Núñez, I. Dienava-Verdoold, E. Herczenik, K. Mertens, A. B. Meijer, *J. Thromb. Haemost.* **2012**, *10*, 1929; b) N. Wohner, P. Legendre, C. Casari, O. D. Christophe, P. J. Lenting, C. V. Denis, *J. Thromb. Haemost.* **2015**, *13*, 815.
[26] S. Muro, C. Garnacho, J. A. Champion, J. Leferovich, C. Gajewski, E. H. Schuchman, S. Mitragotri, V. R. Muzykantov, *Mol. Ther.* **2008**, *16*, 1450.
[27] L. Hosta-Rigau, P. Schattling, B. M. Teo, M. E. Lynge, B. Stadler, *J. Mater. Chem. B* **2014**, *2*, 6686.
[28] M. E. Lynge, R. Ogaki, A. O. Laursen, J. Lovmand, D. S. Sutherland, B. Städler, *ACS Appl. Mater. Interfaces* **2011**, *3*, 2142.

Received: July 16, 2015
Revised: December 19, 2015
Published online: February 8, 2016